Structure Determination of Mg_5Si_6 Particles in Al by Dynamic Electron Diffraction Studies

H. W. Zandbergen,* S. J. Andersen, J. Jansen

Precipitation hardening, in which small particles inhibit the movement of dislocations to strengthen a metal, has long been used to improve mechanical strength, especially of aluminum alloys. The small size of precipitates and the many possible variants of the orientation relation have made their structural determination difficult. Small precipitates in commercial aluminum-magnesium-silicon alloys play a crucial role in increasing the mechanical strength of these alloys. The composition and structure of the β'' phase in an aluminum-magnesium-silicon alloy, which occur as precipitates (typically 4 nanometers by 4 nanometers by 50 nanometers) and are associated with a particularly strong increase in mechanical strength, were determined. Element analysis indicates that the composition is Mg_5Si_6. A rough structure model was obtained from exit waves reconstructed from high-resolution electron microscopy images. The structure was refined with electron nanodiffraction data (overall R value of 3.1 percent) with the use of a recently developed least squares refinement procedure in which dynamic diffraction is fully taken into account.

Pure metals are in general rather soft. For example, Al and Fe have a strength of 40 to 70 MPa, depending on grain size, stress level (which reflects, among other things, the dislocation density), and solutes in the matrix, whereas tool steel has a strength of 800 to 1400 MPa. For common applications, most pure metals are too soft, and for many centuries research has been focused on methods to increase the strength of metals. The methods used to obtain this result can be divided into a few groups, including cold working, solid solution hardening, and precipitation hardening.

Cold working and solid solution hardening have been used since ancient times. Research on precipitation hardening started at the beginning of this century with the discovery of Al-Cu alloys and Wilm's research (*1*) on the strength of Al-Mg alloys. With precipitation hardening, small amounts of other elements are added that form precipitates during a specified temperature cycle. Commonly used precipitation-hardened Al alloys are the binary systems with Cu and Ag and the ternary systems with Mg and Zn (Al-Mg-Zn) and with Mg and Si (Al-Mg-Si). Typically, the alloying agents are present at roughly 0.5 weight %.

The common procedure is to bring the alloy to a high temperature so as to dissolve all of the added elements, after which it is cooled quickly to room temperature, thus forming a supersaturated solid solution. When kept at a reasonably low temperature (typically 150° to 250°C for the Al alloys), the materials increase in strength because of precipitation from a supersaturated solid solution. In the case of the Al-Si-Mg alloy, precipitation hardening can triple or quadruple the strength. The strength-time curve shows a maximum at some aging time. Usually, the materials are just slightly underaged, which means that aging (precipitation hardening) is stopped just before maximum is reached. Evidently the strict requirements on the aging temperature and time set restrictions to the further processing of precipitation-hardened materials. Excessive heating should be prevented; thus, welding is usually not performed on such materials or the precipitation hardening is done after the welding. For instance, the wings of airplanes are mostly put together with rivets for this reason.

Controlling Dislocation Movement

The relatively low strength of pure metals is due to the ease with which dislocations can move through the material. The increase in strength of precipitation-hardened metals is governed by the interaction of moving dislocations with the precipitates. Obstacles for dislocations are the precipitate itself and the strain connected with the precipitate. The strain field around a precipitate is largest when the lattices of the precipitates are coherent or semicoherent, which implies that across the matrix interface the lattice planes continue with no dislocations (coherent) or a few dislocations (semicoherent). In the case of an incoherent precipitate, the strain field is small, and thus the pinning potential of this precipitate is relatively small. Therefore, one tries to form coherent or semicoherent precipitates in the precipitation hardening. Evidently, knowledge of the interface and the orientation relations of the precipitates with the matrix is essential for an understanding of the strength enhancement.

In general, the precipitates should be small and occur with a high density. The reason for this requirement is that the dislocation can curve around the precipitate and its stress field. Thus, it is important that the spacings between the particles are small so that the neighboring precipitates hinder dislocations to curve. In the Al-Si-Mg alloy that we studied, the density of precipitates is ~10,000 precipitates/μm^3, which is slightly more than 20 precipitates/μm, that is, somewhat less than 50 nm of separation. This distance is about 250 atomic spacings, which will limit dislocation glide considerably.

Properties of Precipitation-Hardened Alloys

The corrosion properties of a precipitation-hardened alloy can be quite different from the pure metal, because the precipitates usually have a different chemical formula than the matrix. The Al-Mg-Si system has very good corrosion properties; one assumes that this is more related to the elements that were added than to the formation of precipitates per se. However, the size of the precipitates is quite important. As long as a homogeneous material with small precipitates is obtained, large chemical potential gradients do not arise and the material is reasonably corrosion resistant. Thus, just as for strength enhancement, for corrosion resistance it is beneficial to have very small precipitates.

In corrosion resistance as well as in fracture toughness, grain boundaries play a crucial role, in particular, because the areas near the grain boundaries show a different precipitation hardening. Near grain boundaries the density of vacancies is much lower than in the matrix, because grain boundaries act as vacancy sinks. The vacancies play a crucial role in the atom diffusion that is necessary for the

---

H. W. Zandbergen is at the National Centre for High Resolution Transmission Electron Microscopy (HREM), Laboratory of Materials Science, Delft University of Technology, Rotterdamseweg 137, 2628 AL Delft, Netherlands. S. J. Andersen is at the National Centre for HREM, Laboratory of Materials Science, Delft University of Technology, Rotterdamseweg 137, 2628 AL Delft, Netherlands, and Senter for Industriell og Teknisk Forskning Applied Physics, 7034 Trondheim, Norway. J. Jansen is at the National Centre for HREM, Laboratory of Materials Science, Delft University of Technology, Rotterdamseweg 137, 2628 AL Delft, Netherlands, and the Laboratory for Crystallography, University of Amsterdam, Nieuwe Achtergracht 166, 1018 WV Amsterdam, Netherlands.

*To whom correspondence should be addressed.

formation of the precipitates. Because of the vacancies, the diffusion can be several orders of magnitude faster than for a material without vacancies. The lower vacancy concentration near the grain boundaries allows the formation of precipitation-free zones (PFZs) near the grain-boundary areas, which leads to different chemical potentials and thus greater corrosion. For example, the PFZs in the 7xxx (Al-Mg-Zn) alloys can be prone to stress corrosion cracking, and the solutes in the PFZs make the grain boundaries more brittle. A process called retrogression and re-aging, which is a very brief aging (above 200°C for some minutes) and a subsequent re-aging at (for example, 120°C for 10 hours), is therefore often used to induce nucleation in these boundaries.

The property most affected by the precipitation is the electrical resistivity. Aluminum has many applications because it is both light and a good electrical conductor. The resistivity of the supersaturated solid solution Al-Si-Mg alloy is greater because of the Mg and Si atoms, which scatter the electrons. The resistivity usually increases upon hardening and is often high when the material has maximum hardness, after which the resistivity decreases again. Thus resistivity, which is readily measured, is often used as a means of assessing quality in these alloys. It is also used to study the formation of the different phases.

The β'' Phase in Al-Mg-Si Alloys

In Al-Mg-Si alloys (about 0.5 weight % Mg and 0.5 weight % Si), a strong increase in the strength is caused by precipitates formed during temperature treatments. Upon annealing of the Al-Mg-Si alloy at about 200°C, the dissolved Mg and Si precipitate; with increasing annealing time, a sequence of phases that increase in size is formed. The maximum hardness in these alloys is obtained when the alloys contain a combination of very small Guinier Preston (GP-I) zones (*2*) with diameters of ~2.5 nm and larger needles of a phase that is called β'' (*3–5*) with a typical size of 4 nm by 4 nm by 50 nm. The number 3-5 density of these precipitates is high; for the β'' phase needles, a number density of 10^4/mm^3 is typical and corresponds to a volume fraction of only nearly 1%. The GP-I zones are assumed to be strongly enriched in Si and Mg and to have a structure similar to that of the surrounding Al matrix, whereas the β'' phase has a different structure. The monoclinic unit cell of β'' is reported (*4*) to have the cell dimensions $a = 1.53(1)$ nm, $b = 0.405$ nm, $c = 0.67(2)$ nm, $\beta = 106(2)°$ (values in parentheses are standard deviations).

The structures of the various phases in the high-strength alloy must be determined if the mechanisms of strength enhancement are to be understood. However, the small size of the β'' precipitates, their low volume fraction, and their occurrence in 24 orientations in the Al matrix do not allow conventional structure determination (for example, by x-ray and neutron diffraction). Conventional high-resolution transmission electron microscopy (HREM) also does not provide sufficient detail to elucidate the structure. Therefore, we applied two recently developed techniques: (i) exit wave reconstruction from a through-focus series of HREM images (*6, 7*), which was used to construct a rough structure model, and (ii) a least squares structure refinement (*8*) that uses electron diffraction data and takes dynamic diffraction fully into account. Dynamic diffraction results from multiple scattering of the same electron within the specimen. Dynamic diffraction occurs for electrons even in very thin crystals because the electron-matter interaction is very strong (about 10^5 times as large as that for x-rays). The dynamic diffraction results in changes in the relative intensities of the reflections as a function of the specimen thickness. Therefore, kinematic diffraction, which is valid for almost all x-ray and neutron diffraction, cannot be applied. As shown in this article, the inclusion of dynamic scattering in the refinement procedure leads to much more reliable results, in particular for specimen thickness above 10 nm.

Experimental Methods and Analysis

A commercial Al-Mg-Si alloy (*9*) was thinned to sufficient electron transparency (thickness < 40 nm) by electropolishing. Electron microscopy was performed with a Philips CM30ST-FEG electron microscope that has an information limit for HREM images of 0.14 nm (*10*). The microscope sets no information limit to the electron diffraction data because the intensities of the reflections are not influenced by the microscope aberrations. The information limit in diffraction space is mainly restricted by the specimen (related to the thickness and thermal vibrations of the atoms). Partly to reduce the thermal vibrations, the specimen was cooled to about 100 K for the electron diffraction recordings (*11*). The information limit in the diffraction patterns is about 0.07 nm. Electron diffraction was performed with spot sizes between 6 and 10 nm. The refinements were done with the recently developed software package Multi-Slice Least Squares (MSLS) (*8*), in which multislice calculation software is combined with least squares refinement software used in x-ray crystallography. In multislice calculations, which are routinely used for image calculations of HREM images, dynamic diffraction is taken into account explicitly. The MSLS package is described in detail in (*8*). The R value used in the refinements was $\Sigma(I_{\text{obs}} - I_{\text{calc}})^2/\Sigma I_{\text{obs}}^2$ (*12*), which uses only the significant reflections (*12*).

Energy dispersive x-ray (EDX) element analysis (*13*) of about 50 β'' precipitates indicates a Mg/Si atomic ratio of about 0.8. Some precipitates showed a considerably higher Mg/Si ratio. Such a high ratio is in agreement with the presence of another phase, β' (*14, 15*), which is observed in some precipitates and which occurs predominantly at the interface between β'' and the Al matrix (*15*).

The through-focus exit wave reconstruction (TFEWR) uses the focus dependence of the image distortion by the electron microscope to correct for this distortion. With the use of algorithms developed by Coene *et al.* (*16*), all useful information is extracted from a series of HREM images taken at different defocus values with known focus increments. The result is the exit wave function that contains amplitude as well as phase information up to the information limit of the microscope. The exit wave function, or exit wave for short, is the electron wave at the exit plane of the specimen. A major advantage of the exit wave is that the information, which is delocalized (*17*) in the HREM images, resulting in a blurred image (Fig. 1A), is restored to its origin (Fig. 1B). In addition to the advantage of the deblurring, the noise level of the exit wave is less than for a single image because 15 to 20 HREM images are used for the reconstruction.

A reconstructed exit wave (*18*) of a β'' precipitate embedded in Al is shown in Fig. 1B. The viewing direction is along the [100] zone axis of Al and the [010] direction, $\mathbf{b}_{\beta''}$, of the β'' particle, which is along the needle. HREM images perpendicular to $\mathbf{b}_{\beta''}$ have shown a good lattice match between β'' and the Al matrix along the needle direction. On the other hand, in the directions perpendicular to $\mathbf{b}_{\beta''}$, misfit dislocations occur at the β''-Al interface (*19*). To enhance the visibility of these dislocations, we Fourier filtered the image of Fig. 1B, omitting all reflections except for the Al reflections and their immediate surroundings (using apertures as shown in Fig. 1C). The resulting image is shown in Fig. 1D, in which the dislocations are indicated with arrows. The dislocations at the β''-Al interface are related to the mismatch between both lattices. This mismatch is 3.8% along the a axis and 5.3% along the c axis. Along the b axis of β'', no mismatch occurs.

Structural Refinement

From a magnified part of Fig. 1B (Fig. 2), a trial model for the structure refinement was obtained in the following way. From the coherency of the interface between the β'' particle and the Al matrix, it was concluded that the Si and Mg atoms are located at or close to the $y = 0$ and $y = 1/2$ planes. From the unit cell volume, it was concluded that the number of atoms in the unit cell is 22. When the Mg/Si ratio as determined by EDX element analysis is taken into account, it follows that the composition is probably Mg_5Si_6. Next, atoms were placed at the dark spots in the exit wave image. The darkest spots were assumed to be two Si atoms in different layers, which are so close together in projection that they merge into one spot. The dark spot with the largest distances to the other black dots (chosen as the corner of the unit cell) was assumed to be Mg, because Mg has a larger radius (0.155 nm) than Si (0.115 nm). The remaining Mg and Si atoms were assigned to the other black dots on the basis of the radii of Mg and Si. The resulting estimated atom positions are given in Table 1.

We used the model deduced from the reconstructed exit wave as the starting model for the MSLS refinement employing simultaneously seven electron diffraction data sets along [010] or [001]. These data were collected from β'' particles containing no defects, because the presence of defects results in streaking or extra peaks, similar to those in Fig. 1C. Because the electron diffraction data were recorded from areas containing β'' and the Al matrix, the Al reflections and about 10% of the β'' reflections were omitted (*20*). The overall *R* value of the starting model was 15%. The refinements were done in space groups C2/m, C2, Cm, and C1, which were suggested by the systematically absent reflections (*21*). The refinements in the lower symmetric space groups did not lead to significantly better fits nor to different atom positions, indicating that the space group is C2/m. The resulting atomic parameters are given in Table 1. The overall *R* value after refinement was 3.1%. Table 2 lists the number of reflections, the refined crystal misorientation, and the *R* values of each diffraction pattern.

Table 2 also gives the *R* values when only kinematic diffraction is taken into account (*22*). Obviously, for the thicker specimen areas, these *R* values are much higher than those obtained by the inclusion of dynamic diffraction. This indicates that even for a material like Mg_5Si_6 with only light elements, the dynamic diffraction is very significant for small specimen thicknesses (about > 10 nm). Consequently, it is important to include the dynamic scattering in the structure refinement. Moreover, the use of diffraction data from areas with different thicknesses adds substantially to the reliability of the structure refinement.

The refined thicknesses are in good agreement with the shape of the β'' precipitates. The β'' precipitates are quite long along the *b* axis (about 50 nm), and therefore the thickness will be mostly determined by the specimen thickness, which can vary from place to place. Indeed, the thicknesses of the [010] diffraction data sets were refined to values between 7 and 22 nm. On the other hand, the β'' precipitates are about 4 nm thick perpendicular to the *b* axis, and therefore one also expects such a result from the refinement of the [001] diffraction data, as is indeed observed. Because the specimen is likely to be thicker than 4 nm, the β'' particle is embedded in the Al

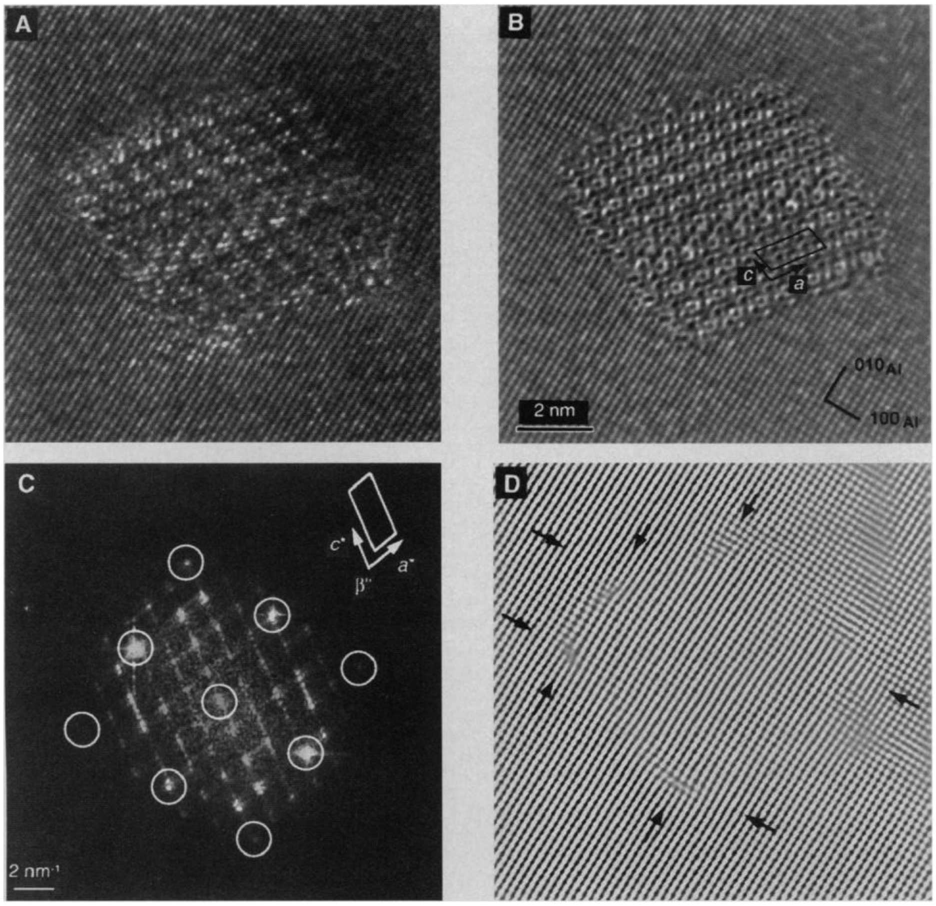

Fig. 1. (**A**) Experimental HREM image, which is the first (defocus is about −70 nm) of the series of 20 images used for the reconstruction of the exit wave given in (**B**), which shows the phase of the exit wave; the amplitude of the exit wave is quite similar and is therefore not shown. (**C**) Fourier transform of the exit wave. (**D**) Exit wave after Fourier filtering. For the Fourier filtering, the reflections of Al and their surroundings [outlined by the circles in (C)] were passed and all other information (and thus all β'' superreflections) was deleted. Because the Al reflections coincide with some β'' reflections, the β'' lattice has about the same appearance as that of Al. The Fourier filtering improves the visibility of the misfit dislocations at the β''-Al interface [indicated by arrows in (D)]. The β'' unit cell is indicated in (B). Because of the *C* centered symmetry, the *a* axis is twice the apparent periodicity. The unit cell parameters estimated from this and other exit waves are $a = 1.516(2)$ nm, $b = 0.405$ nm, $c = 0.674(2)$ nm, and $\beta = 105.3(5)°$, which are in agreement with those reported by Edwards *et al.* (*4*). Because the length of the *b* axis of β'' is equal to that of Al and the latter is used for the calibration of the magnification, no standard deviation for the *b* axis is given.

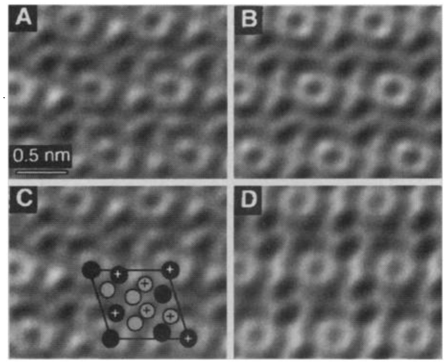

Fig. 2. (**A**) Part of the reconstructed exit wave (phase) of the β'' structure from Fig. 1B. (**B**) The same exit wave, but after we averaged over four unit cells and imposed *C*2/*m* symmetry by image processing. (**C**) The same exit wave as in (A) but with an overlay of the atoms as deduced from the exit wave (Mg, black atoms; Si, grey atoms; + indicates an atom at $y = 1/2$). (**D**) Calculated exit wave (phase) that uses the refined atomic positions from Table 1.

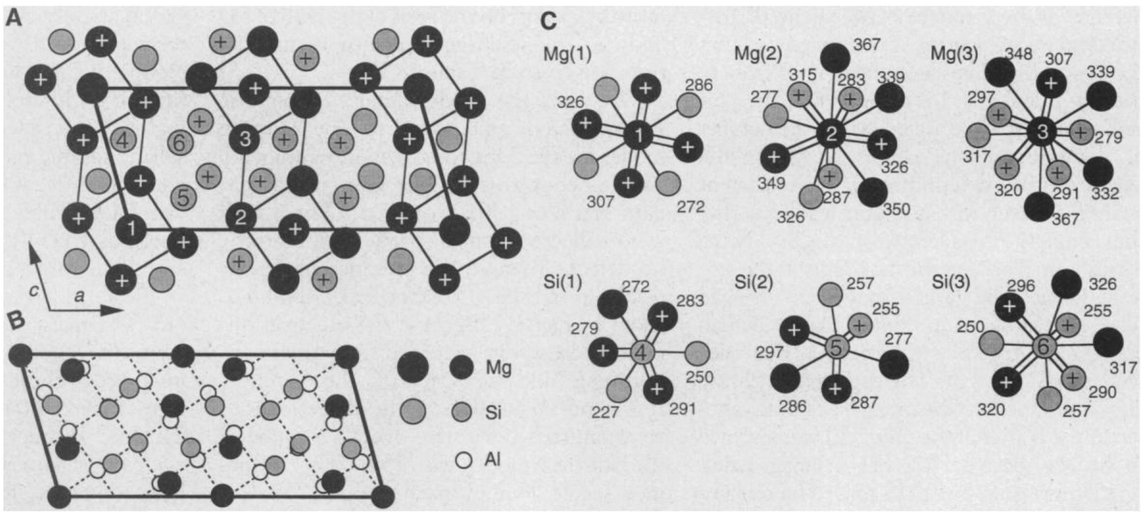

Fig. 3. (**A**) Schematic representation of the structure of β" Mg_5Si_6 viewed along the *b* axis. Atoms are at *y* = 0 or *y* = 1/2 (the latter is indicated by +). (**B**) Overlay of the atoms of the β" structure with the Al lattice (which is slightly expanded to fit to the β" unit cell). The atoms in the β" structure are at the same height as those in the Al lattice, except for the atom Mg(1), which is shifted over half the *b* axis. The coordinations of the six different atoms are given in (**C**), with atomic distances to the central atom in picometers. The standard deviation of these distances is 3 pm or less.

matrix along the electron beam direction. This should lead to some "cross talk" between the Al and β" reflections (*23*), which will result in additional changes in the intensities and thus larger *R* values.

Three types of atom coordinations occur in the β" structure (Fig. 3): (i) a four-capped cube-like surrounding for Mg(1) and Si(6), resulting in a 12 coordination; (ii) a 15 coordination with a pentagonal-like shape for Mg(2) and Mg(3); and (iii) a tricapped trigonal prism for Si(4) and Si(6), resulting in a nine coordination. The interatomic distances agree quite well with those of the known structures of Mg, Si, and Mg_2Si. The Mg-Mg, Si-Si, and Mg-Si distances in these compounds are 0.320, 0.235, and 0.277 nm, respectively, whereas the shortest distances found for Mg_5Si_6 are 0.307(2) for Mg-Mg, 0.227(2) nm for Si-Si, and 0.260(2) nm for Mg-Si. The interatomic distances are consistent with a composition of Mg_5Si_6 as indicated by the EDX element analysis. Given the interatomic distances and the different sizes of Mg and Si, a substantial degree of disorder is unlikely.

Table 1. Atomic positional parameters in fractional values *x*, *y*, and *z* and isotropic temperature factors, *B*, for Mg_5Si_6, with *a* = 1.516(2) nm, *b* = 0.405 nm, *c* = 0.674(2) nm, β = 105.3(5)° and space group *C*2/*m*. For the positions estimated from the exit wave, two values are given, because of the absence of a twofold symmetry in this exit wave. The values given in parentheses in the *x*, *z*, and *B* columns are the standard deviations.

Atom	Estimated from exit wave		Refined by MSLS			
	x	*z*	*x*	*y*	*z*	*B*
Mg(1)	0	0	0	0	0	0.5(2)
Mg(2)	0.35, −0.33	0.06, −0.08	0.3459(8)	0	0.089(2)	1.0(2)
Mg(3)	0.37, −0.43	0.57, −0.63	0.4299(10)	0	0.652(3)	0.8(2)
Si(1)	0.06, −0.06	0.66, −0.65	0.0565(7)	0	0.649(2)	1.1(2)
Si(2)	0.18, −0.18	0.25, −0.26	0.1885(8)	0	0.224(2)	0.5(2)
Si(3)	0.19, −0.21	0.60, −0.61	0.2171(9)	0	0.617(2)	2.5(4)

Table 2. Data on the diffraction sets used for the refinement of Mg_5Si_6 listed in Table 1. We obtained the kinematic *R* values after refinement of only the scale factors, keeping all other parameters fixed and using occupancies of only 1% (*23*). The crystal misorientation is given as the position of the projection of the center of the Ewald sphere in Miller indices *h*, *k*, and *l*.

Zone	Number of observed reflections	Thickness (nm)	Crystal misorientation			R value (%)	
			h	*k*	*l*	MSLS	Kinematic
[010]	50	6.7(5)	8.3	0	−2.3	3.0	3.7
[010]	56	15.9(6)	2.6	0	−1.8	4.1	8.3
[010]	43	16.1(8)	−1.7	0	0.3	0.7	12.4
[010]	50	17.2(6)	−5.0	0	−1.0	1.4	21.6
[010]	54	22.2(7)	−5.9	0	2.5	5.3	37.3
[001]	72	3.7(3)	−3.9	4.5	0	4.1	4.5
[001]	52	4.9(6)	3.6	−1.9	0	6.8	9.3

The atom positions obtained from the TFEWR are similar to the positions obtained from the MSLS refinement. The largest difference in atom position is 0.08 nm. The calculated exit wave (*24*) is in reasonable agreement with the experimental one, as can be seen from Fig. 2, A, C, and D. An important difference is that the experimental exit wave does not show the C2/m symmetry. This is at least in part due to a misorientation of the specimen, which is also evident from the surrounding Al matrix. It can furthermore be caused by residual aberrations of the microscope (such as threefold and twofold astigmatism and beam tilt). A loss of symmetry is observed very frequently in HREM images. Applying the C2/m symmetry to the experimental image (Fig. 2B) gives a better fit between the experimental and calculated exit waves.

The orientation relation of the β" precipitate with the Al matrix (*25*) can be seen in Fig. 3B. The atoms in β" are shifted with respect to the atom positions in the Al basic lattice, mainly to accommodate for the size difference of Mg and Si. A refinement started with the Al positions resulted in an overall R value of 16%, which indicates the usefulness of the reconstructed exit wave to determine a proper starting model.

In this structure refinement of Mg_5Si_6, dynamic diffraction was fully taken into account, allowing the accurate elucidation of an unknown structure, in particular by the use of data sets from various orientations and thicknesses. Because the crystal misorientation is also refined, a mistilt can be used to enhance the resolution in certain directions in diffraction space. The results from the MSLS refinement are more reliable than those from the TFEWR (and HREM), because the diffraction information extends about twice as far (0.14 nm for TFEWR versus 0.07 nm for electron diffraction) and because the diffraction information is not changed by the electron microscope aberrations. Therefore, we did not try to get the best fit between the experimental and the calculated exit waves. The *R* values obtained are very low compared with the *R* values of electron diffraction refinements reported in the literature (*26*). The lower *R* values result mainly from the inclusion of dynamic diffraction in our refinements, indicating the necessity for taking the dynamic diffraction into account. The structure of Mg_5Si_6 is very likely to be correct given the low *R* values obtained, the fit of the experimental and calculated exit waves, and the plausible interatomic distances and coordinations obtained for all atoms.

REFERENCES AND NOTES

1. A. Wilm, *Metall. Z. Ges. Höttenkunde* **8**, 225 (1911).
2. A. H. Geislet and J. K. Hill, *Acta Crystallogr.* **1**, 238 (1948).
3. G. A. Edwards, K. Stiller, G. L. Dunlop, *Appl. Surf. Sci.* **76/77**, 219 (1994).
4. G. A. Edwards, G. L. Dunlop, M. J. Couper, in *Proceedings of the International Conference on Aluminum Alloys*, Georgia Institute of Technology, Atlanta, GA, 11 to 16 September 1994 (Georgia Institute of Technology, Atlanta, 1994), p. 620.
5. S. J. Andersen, *Met. Mater. Sci.* **26A**, 1931 (1995).
6. D. Van Dyck and M. Op De Beeck, in *Proceedings of the 12th International Congress on Electron Microscopy*, International Federation of Electron Microscope Societies, Seattle, WA, 12 to 18 August 1990 (San Francisco Press, Seattle, WA, 1990), pp. 26–27.
7. W. Coene, G. Janssen, M. Op De Beeck, D. Van Dyck, *Phys. Rev. Lett.* **69**, 3743 (1992).
8. J. Jansen, D. Tang, H. W. Zandbergen, H. Schenk, in preparation. MSLS uses a standard algorithm to minimize the *R* value. To determine the gradient of the *R* value as a function of the thickness, we added a very thin slice at the exit plane of the multislice calculation. To determine the accuracy of MSLS, we applied it on several compounds with known structures (LaNiBN, $La_3Ni_2B_2N_3$, $Ce_5Cu_{19}P_{12}$, $Ba_2Ca_3Cu_5O_{10}$, and $Ba_2Ca_2Cu_4O_8$) determined by x-ray single-crystal diffraction or neutron powder diffraction. The MSLS refinement resulted in very similar (a difference in atom positions less than 0.01 nm and on average less than 0.003 nm) atom positions. Putting one or more atoms at the wrong position gives much higher *R* values.
9. The material investigated was Al with 0.2 weight % Fe, 0.5 weight % Mg, 0.53 weight % Si, and 0.01 weight % Mn, extruded as described in (*5*) and aged at 185°C for 5 hours.
10. The information limit is not circular but elliptical (0.135 nm by 0.150 nm), because of the anisotropic response of the microscope to external vibrations.
11. Other reasons to cool the specimen are the reduction of the electron beam induced contamination and amorphization. Unfortunately, commercial sample cooling holders do not allow real HREM imaging; thus it is difficult to do electron diffraction and HREM on the same precipitates.
12. I_{obs} and I_{calc} are the intensities of the reflections. The significant reflections are $I_{obs} > 2\sigma(I_{obs})$, where $\sigma(I_{obs})$ is the standard deviation of the reflection.
13. EDX element analysis was done with a Link EDX element analysis system, and the mineral forterite was used to calibrate the Cliff-Lorimer factor for these two elements.
14. K. Matsuda, S. Tada, S. Ikeno, T. Sato, A. Kamio, *Scr. Mater.* **32**, 1175 (1995).
15. S. Andersen *et al.*, in preparation.
16. W. Coene, A. Thust, M. Op De Beeck, D. Van Dyck, *Ultramicroscopy* **64**, 107 (1996).
17. The frequency-dependent delocalization or information shift, *S*, of the shape has been described in (*27*) and is $S = \varepsilon\lambda\mathbf{g} + C_s\lambda^3\mathbf{g}^3$, where ε is the defocus, λ is the wavelength, C_s is the spherical aberration, and **g** is a reciprocal lattice vector. For instance, for a 300-keV microscope with a point-to-point resolution of 0.2 nm ($C_s = 1.2$ mm) at Scherzer focus (optimal focus) (−60 nm), *S* of the 0.1-nm frequency ($\mathbf{g} = 10$ nm^{-1}) is 8.4 nm, and *S* is 0.6 nm and −0.04 nm for the 0.2-nm frequency ($\mathbf{g} = 5$ nm^{-1}) and 0.3 nm ($\mathbf{g} = 3.33$ nm^{-1}) frequency, respectively.
18. For the TFEWR, series of 20 HREM images were recorded with focus increments of 5.2 nm. The starting focus was about −70 nm. The images were recorded with a 1024 by 1024 pixel slow scan charge-coupled device camera.
19. Further analysis of this exit wave, such as the atomic structure at the interface between β" and the Al matrix and the structure and the origin of the defect in the β" precipitate, is given elsewhere (*15*).
20. Because of the overlap with the Al reflections, the 10% discarded reflections are rather random for the structure of the precipitate, which implies that the accuracy of the structure determination is not substantially hampered by this omission.
21. The space group could have been determined by convergent beam electron diffraction, but given the small size of the precipitates, this method was not used.
22. To approximate a kinematic refinement with the MSLS program, a very small thickness (for example, 1 nm) or a very low occupancy should be used. The latter approach was used because in this way the excitation error of the diffraction spots is properly taken into account. This excitation error occurs because, in contrast with x-ray single-crystal diffraction in which each diffracted beam is measured at its maximum (reflections are in exact Bragg condition), most diffracted beams in electron diffraction are not in exact Bragg condition. In the calculation of the kinematic *R* values, a 1% occupancy of all atom sites and the thicknesses obtained for the dynamic refinement were used.
23. It would be better to do a complete refinement with the addition of an Al matrix in front and after the precipitate and to refine the thicknesses of these two layers as well. This, however, is not yet possible with the MSLS package.
24. For the simulated exit wave, the following parameters were used: defocus spread, 10 nm, which is used to impose an information limit of about 0.14 nm; specimen thickness, 10 nm; convergence angle, 0.1 mrad; and crystal tilt, 1.5° about the $[20\bar{1}]$ direction. The specimen tilt and thickness were roughly estimated from the loss of symmetry in the surrounding Al matrix. The agreement between the calculated and the experimental exit wave can be improved by adjustment of the twofold astigmatism and beam tilt, but this would be merely a cosmetic improvement without giving any proof of the reliability of the model.
25. The orientation relation is $[100]_{\beta''}//[230]_{A1}$, $[010]_{\beta''}//[001]_{Al}$, and $[001]_{\beta''}//[310]_{Al}$.
26. D. L. Dorset, *Structural Electron Crystallography* (Plenum, New York, 1995).
27. W. Coene and A. J. E. M. Jansen, *Scanning Microsc. Suppl.* **6**, 379 (1992); H. W. Zandbergen, D. Tang, D. Van Dyck, *Ultramicroscopy* **64**, 185 (1996).

28. The Al-Mg-Si specimen was supplied by HYDRO Aluminum AS (Sunndalsøra, Norway). Stichting Technische Wetenschappen is acknowledged for financial support. We thank D. van Dyck and M. op de Beeck for discussions. S.J.A. is indebted to Norsk Hydro Al for financial support.

Competing Interactions and Levels of Ordering in Self-Organizing Polymeric Materials

M. Muthukumar, C. K. Ober, E. L. Thomas

The sophisticated use of self-organizing materials, which include liquid crystals, block copolymers, hydrogen- and π-bonded complexes, and many natural polymers, may hold the key to developing new structures and devices in many advanced technology industries. Synthetic materials are usually designed with only one structure-forming process in mind. However, combination of both complementary and antagonistic interactions in macromolecular systems can create order in materials over many length scales. Here polymer materials that make use of competing molecular interactions are summarized, and the prospects for the further development of such materials through both synthetic and processing pathways are highlighted.

Structural order over many length scales can be created in self-organizing materials by the presence of several molecular interactions including (i) hydrophobic and hydrophilic effects, (ii) hydrogen bonding, (iii) coulombic interactions, and (iv) van der Waals forces (*1*). The idea of combining interactions in the design of new synthetic macromolecular materials is just starting to be explored systematically. Within this framework, polymer scientists are currently attempting to bridge the extremes of the precision and elegant complexity of many biological materials and the statistical nature and relative simplicity of most synthet-

---

M. Muthukumar is in the Department of Polymer Science and Engineering, University of Massachusetts, Amherst, MA 01003–4530, USA. C. K. Ober is in the Department of Materials Science and Engineering, Cornell University, Ithaca, NY 14853-1501, USA. E. L. Thomas is in the Department of Materials Science and Engineering, Massachusetts Institute of Technology, Cambridge, MA 02139-4307, USA.